Tenth International Conference on Computational Fluid Dynamics (ICCFD10), Barcelona,Spain, July 9-13, 2018

ICCFD10-2018-0236

Investigation of gravity-driven inertial particles clusters and their locations in turbulence structure using Kinematic simulation

M. Farhan*,**, F.C.G.A. Nicolleau**, M.S. Kamran *, M. Farooq *and I.A. Chaudry *
Corresponding author: m.farhan@uet.edu.pk

* Department of Mechanical Engineering, University of Engineering and Technology Lahore.
** Sheffield Fluid Mechanics Group, The University of Sheffield United Kingdom

Abstract: We study the clustering of inertial particles in relation to turbulent flow structure in the presence of gravity using Kinematic simulation (KS). The inertial particle clusters are characterized using Stokes number and Froude number ranging $0 \leq St \leq 1$ and $0.4 \leq Fr \leq 1.4$. Turbulent flow predominately consists of vorticity structures is defined by Eulerian velocity field and these vortices are identified by using Q-criterion. In the end, the particles' clusters are located within the isosurfaces of vorticity structure based on different values of Stokes and Froude numbers.

Keywords: Turbulence Structures, Particles' Clusters, Kinematic Simulation.

1 Introduction

In the last decades, the clustering of inertial particles in turbulent flow is the subject of various studies [1, 2, 3, 4, 5, 6, 7, 8, 9,]. The particles clustering in a turbulent flow is of key importance for natural as well as for industrial applications. A better understanding of particle-turbulence relationship can help to solve the mysteries of the Universe. In this paper, we focus on the clustering of gravity-driven inertial particles in relation to turbulence structure. Generally, a turbulent flow is considered as a mixture of various vorticity structures. It has been observed that varying vorticity regions are the major cause of preferential concentration of inertial particles in the turbulent flow. Using the experiments, Eaton and Fessler [10] found that the heavier particles are ejected by the vortical structures and develop as a cluster in the low vorticity regions.

Similar settling patterns are also reported in many numerical studies. Q-criterion (a method to identify the vortex regions in turbulent flow) is used to locate particle clustering in the different flow regions such as streaming, eddies, rotational, etc. [11]; they differentiated the concentration levels by plotting the particles number density distributions functions and found that the average concentration of the particles (particularly of the intermediate size) in the strain regions is clearly different from high vorticity regions. An identical trend of clustering for the different sized particles is shown by Wang and Maxey [12] and Bec et al. [13] who identified the preferential clustering of inertial particles using different statistical measures.

Further to this, Calzavarini et al. [14] used the Minkowski functional to describe the ejection of particles from vortices and Q-criterion was used to show that there is no difference in the Q-criterion distributions for fluid tracers and the particles with $St \simeq 3$ [15]. Altogether all of these previous studies confirm the ejection of inertial particles from the vorticity regions and the particles tend to settle in the strain regions based on St.

Most recently, Nilson et al. [16] analyzed the particle clustering in the Gaussian and non-Gaussian synthetic turbulent flows. They found that inertial particles cluster in the local low vorticity regions depending on

Stokes number and it has been reported that the particles with low St cluster as a result of the vortex centrifugal effect in small-scale turbulence.

In the light of above discussion, it is interesting to see the locations of gravity-driven inertial particles' clusters in turbulent flow. For this purpose, we divide this paper into two parts. First, we briefly explain the formation and types of inertial particles Lagrangian attractors and then, their locations are determined in the turbulence structure using visualization and statistical approaches. The paper is organised as follows: in § 2 we introduce the Kinematic Simulation (KS) and development of Lagrangian attractors. The mathematical background related to turbulence structure is discussed in § 3. The results of locations of attractors based on visualization and statistics are explained in § 4 and § 5 respectively. Section 6 summarises our main conclusions.

2 Kinematic Simulation and Lagrangian Attractors

Kinematic Simulation (KS) is a particular case of synthetic turbulence where the focus is on particle's trajectory at the expense of solving the Navier-Stokes equation. An analytical formula 'synthetic flow' is used for the Eulerian flow field. Though the synthetic turbulence retains less information than the whole flow contains, its success relies on keeping what is paramount for the Lagrangian story.

The simplicity of the KS model excludes some features of real turbulent flows but captures the part of the physics which is required to perform Lagrangian particle analysis.

KS modelling has been successfully employed and validated [**?**, 17, 18]. This kind of simulation is much less computing-time consuming than DNS, which is important for the present study where we need to run many cases (more than a 1000 cases for 100 turnover times). Each case corresponds to a given St, Fr, p and time and involves 15625 particles.

With synthetic simulations, one can develop models where turbulence ingredients and complexity can be added step by step helping to understand their respective importance. These synthetic models can be a useful complement to Direct Numerical Simulation. In particular with KS it is possible to play with the spectral law [19] and its consequences in terms of particle's dispersion.

As we are not interested in two-particle dispersion, we limit our study to the scale ratio $k_{imax}/k_{imin} = 9$ [1] used in [8].

In KS, the computational task reduces to the calculation of each particle trajectory. This trajectory is, for a given initial condition, $\mathbf{X}_0$, solution of the differential equation set:

$$\frac{d\mathbf{X}}{dt} = \mathbf{V}(t) \tag{1}$$

$$\frac{d\mathbf{V}}{dt} = \mathfrak{F}(\mathbf{u}_E(\mathbf{X},t),\mathbf{V},t) \tag{2}$$

where $\mathbf{X}(t)$ is the particle's position, $\mathbf{V}(t)$ its Lagrangian velocity and $\mathbf{u}_E$ the analytical Eulerian velocity used in KS. $\mathfrak{F}$ is a function relating the Lagrangian acceleration to the Eulerian and Lagrangian velocities.

In KS $\mathbf{u}_E$ takes the form of a truncated Fourier series, sum of $N_k = N^3$ Fourier modes:

$$\mathbf{u}(\mathbf{x}) = \sum_{i=1}^{N}\sum_{j=1}^{N}\sum_{l=1}^{N} \mathbf{a_{ijl}}\cos(\mathbf{k_{ijl}}.\mathbf{x}) + \mathbf{b_{ijl}}\sin(\mathbf{k_{ijl}}.\mathbf{x}) \tag{3}$$

where $\mathbf{a_{ijl}}$ and $\mathbf{b_{ijl}}$ are the decomposition coefficients corresponding to the wavevector $\mathbf{k_{ijl}}$. In its general form the KS field can also be a function of time but we limit the study to a steady KS.

[1] $i = 1$, 2 or 3

2.1 Periodic KS method for periodic flow

Following [8], the wavevectors $\mathbf{k_{ijl}} = (k_i, k_j, k_l)$ follow an arithmetic distribution to enforce a periodic condition for the velocity flow field:

$$k_i = \frac{2\pi}{L_x}(n_i - 1),\ k_j = \frac{2\pi}{L_y}(n_j - 1),\ k_l = \frac{2\pi}{L_z}(n_l - 1) \tag{4}$$

where (n_i, n_j, n_l) are integers satisfying $1 \leqslant n_i \leqslant N$. In practice, we choose $(L_x = L_y = L_z)$ for creating an isotropic turbulence and to ensure the flow incompressibility the Fourier coefficient vectors $\mathbf{a_{ijl}}$ and $\mathbf{b_{ijl}}$ are set orthogonal to the wavevector:

$$\mathbf{a_{ijl}} \cdot \mathbf{k_{ijl}} = \mathbf{b_{ijl}} \cdot \mathbf{k_{ijl}} = 0 \tag{5}$$

Their magnitude is fixed by the energy spectrum, $E(k)$ (**??**).

$$|\mathbf{a_{ijl}}|^2 = |\mathbf{b_{ijl}}|^2 = 2E(k)\Delta k_{ijl}/m_k \tag{6}$$

where m_k is the number of wavevectors of wavenumber $k = \|\mathbf{k_{ijl}}\|$. This is the key point for using KS for this study. The use of (**??**) in (6) is straightforward and does not require complicated forcing techniques. From the spectral law, the rms velocity (**??**) and the integral length scale can be defined:

$$\mathcal{L} = \frac{3\pi}{4}\frac{\int_{k_{min}}^{k_{max}} k^{-1}E(k)dk}{\int_{k_{min}}^{k_{max}} E(k)dk} \tag{7}$$

The Kolmogorov length scale is defined as $\eta = 2\pi/k_{max}$, whereas the largest physical scale is $L = 2\pi/k_{min}$ which determines the inertial range $[\eta, L]$ over which (**??**) is observed. It is worth noting that $\mathcal{L} \simeq L$ for sufficiently large inertial ranges. However, here in contrast to other KS studies the inertial range is small and $L \simeq 5\mathcal{L}$. In this paper, non-dimensional numbers (St and Fr) are based on the integral length scale $\mathcal{L}$. The ratio between the largest length scale and the Kolmogorov length scale is k_{max}/k_{min} and the associated Reynolds number is: $Re_L = (k_{max}/k_{min})^{4/3}$. This is the standard way to define a Reynolds number in KS and a DNS or an experiment yielding the same ratio k_{max}/k_{min} would have a much larger Reynolds number. Finally, a characteristic time for normalisation can be $t_d = L/u_{rms}$ or $\mathcal{T} = \mathcal{L}/u_{rms}$. The particles are initially homogeneously distributed and whenever a particle leaves the turbulence box domain (e.g. $\mathbf{X}_i > L_x$) it is re-injected from the opposite side to keep the periodic condition.

2.2 Equation of motion

Following [20] the equation of motion for the inertial particle is derived from [21, 22] and consists of a drag force and drift acceleration (weight):

$$\frac{d\mathbf{V}}{dt} = \frac{1}{\tau_a}\left(\mathbf{u}(\mathbf{x}_p(t), t) - \mathbf{V}(t) + \mathbf{V}_d\right) \tag{8}$$

where τ_a is the particle's aerodynamic response time and $V_d = \tau_a \mathbf{g}$ the particle's terminal fall velocity or drift velocity.

2.3 Types of Lagrangian Attractors

The particles initially uniformly distributed in the flow field are allowed to evolve until a Lagrangian attractor is achieved. The shape of the attractor varies from clear one-dimensional structures to three-dimensional distributed structures depending on Stokes number and Froude number. These attractors are categorised as;

i) 1D-H : horizontal one-dimensional Lagrangian attractor as in Fig. 1(a),

ii) 1D-V : vertical one-dimensional Lagrangian attractor as in Fig. 1(c),

iii) 1D-HV : Intermediate one-dimensional Lagrangian attractor as in Fig. 1(b).

iv) 2D-L : two-dimensional vertical curtain-like layer as in Fig. 1(d) (see also [23]).

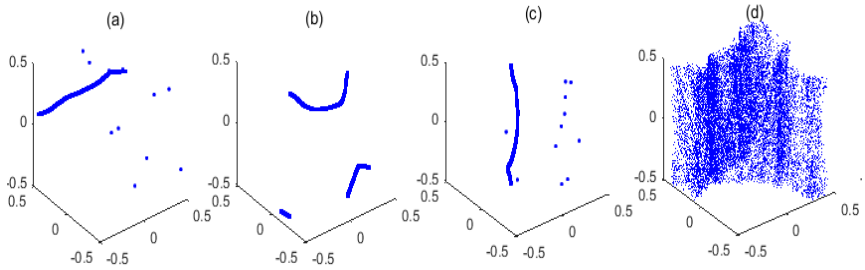

Figure 1: Different characteristic attractor shapes.

3 Mathematical background and definitions

3.1 Vortex detection

A number of vortex detection methods have been developed to identify vortices in the flow and, in general, vortex detection schemes are categorized as follows:

- Vortex regions may be detected on the basis of scalar quantities. For example, the high magnitude of vorticity and positive Q-criterion show the regions of high vorticity in the flow. These approaches can be visualized either by isosurfaces or volume rendering method.
- In the second case of the vortex core detection, instead of regions, the line types features are reduced as high vorticity zones.

Both of these categories can be studied using the established techniques based on different types of applications. As in case of particles' clustering, it is more important to see the regions of high and low vorticity, we focus on the vortex regions techniques for locating the inertial particles' clusters.

3.2 Vortex regions detection methods

There is no clear definition of vortex regions and they are considered as the flow regions with high vorticity or low strain. The models developed to identify the vortex can be based on different flow parameters. Normally, the vortex region quantities are defined by splitting velocity gradient as

$$\nabla u = S + \Omega, \tag{9}$$

i.e., into strain rate tensor (S) and vorticity tensor (Ω) which are also known as symmetrical and anti-symmetrical parts of flow respectively:

$$S = \frac{1}{2}[\nabla u + (\nabla u)^t], \tag{10}$$

$$\Omega = \frac{1}{2}[\nabla u - (\nabla u)^t]. \tag{11}$$

The strain rate tensor (S) measures the stretching and folding in the flow which causes the mixing of particles while vorticity tensor (Ω) is relevant to rotational activities in the flow field. The methods of vortex identification (Q-criterion, λ_2-criterion, $\Delta - criterion$, etc.) are mostly based on the characteristic equation of ∇u;

$$\lambda^3 + P\lambda^2 + Q\lambda + R = 0 \tag{12}$$

where P, Q, and R are the three invariants of velocity gradient ∇u and expressed in terms of symmetric and anti-symmetric flow parts.

3.2.1 Q-criterion

The Q-criterion, also known as Okubo- Weiss criterion, is based on the second invariant of velocity gradient ∇u. It was first used by [24] for three-dimensional flows and mathematically can be expressed as;

$$Q = \frac{1}{2}(\|\Omega\|^2 - \|S\|^2) \tag{13}$$

where the values of Q gives the physical meanings with both positive and negative signs. $Q > 0$ represents the regions of high vorticity while negative values of $Q < 0$ shows the strain dominant regions. The advantage of using this method is easiness of viewing the results by plotting the isosurfaces for both steady and unsteady flow without any serious modification. On the other hand, these isosurfaces are sensitive to the threshold values and it is challenging to pick a right value after a series of iterations.

3.2.2 Vorticity

Vorticity (ω) is defined as the curl of the velocity ($\nabla \times u$) and is twice of the flow rotation at any point. The material element along with ω is stretched by velocity gradient causing the vortex stretching.
where s is the distance along the vortex line. So, the vorticity can be used to identify the vortex based on the region and line methods as classified at the beginning of the section.

Vortex regions are identified directly by using the magnitude of vorticity. But the limitation of this method is not to differentiate between swirling and shearing motions. Similar to Q-criterion, the vorticity is visualized by using the isosurfaces of ω depending on the threshold values of ω.

4 Results and discussion

We use kinematic simulation to identify the locations of inertial particles' clustering using Kolmogorov and non-Kolmogorov energy spectra. The formations and classification of Lagrangian attractors with varying values of Stokes number and Froude number can be found in [8, 9]. In order to develop better positioning of these attractors, we explore their locations within the turbulence structure. First, the visualization approach is used to locate the different types of attractors and then, a statistical approach is used to confirm the positioning.

4.1 Locations of attractors with Kolmogorov Energy Spectrum

We develop the relationship of Lagrangian attractors with vortex regions of turbulent flow using Q-criterion. In practice, the velocity components are used to find the velocity gradients and hence to calculate the Q-criterion. The results of Q-criterion are plotted as isosurfaces using an appropriate threshold value. A combined isosurface plot in Fig. 2 representing the high vorticity regions as green isosurfaces ($Q > 0$) and the low vorticity regions as blue isosurfaces ($Q < 0$) for Kolmogorov energy spectrum ($P = 5/3$).
After attempting a number of Q-criterion values, the major task is to choose a reasonable threshold value so that we may able to see the attractors' locations within the isosurfaces. In order to do this, we plot the isosurfaces using different threshold values to see the exact location of an attractor. As a result of our investigation, we locate the different type of Lagrangian attractors with the threshold value of $iso_Q = \pm 180$. Following the results of past studies i.e. inertial particles are normally centrifuged by high vorticity regions and they preferably settle in the strain regions, we emphasize the position of present two different one-dimensional (1D-H and 1D-V) along with isosurfaces in Fig. 3 and Fig. 4 respectively. It can be observed that both one-dimensional attractors develop in the low vorticity regions for Kolmogorov energy spectrum.

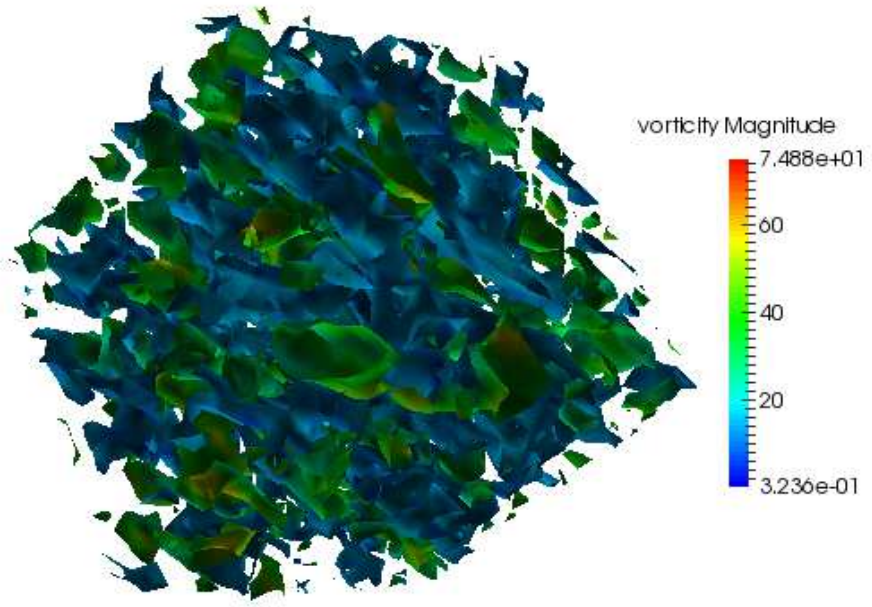

Figure 2: Vorticity regions isosurfaces (green) for Q=180 and Strain regions (blue) isosurfaces for Q=-180 with $p = 5/3$

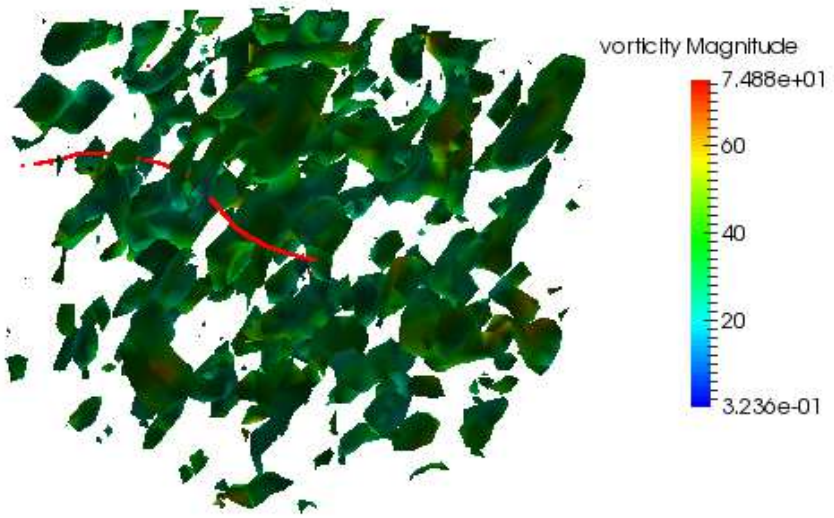

Figure 3: Location of 1D-H attractor (St=0.207 and Fr=1.10) in flow with $p = 5/3$

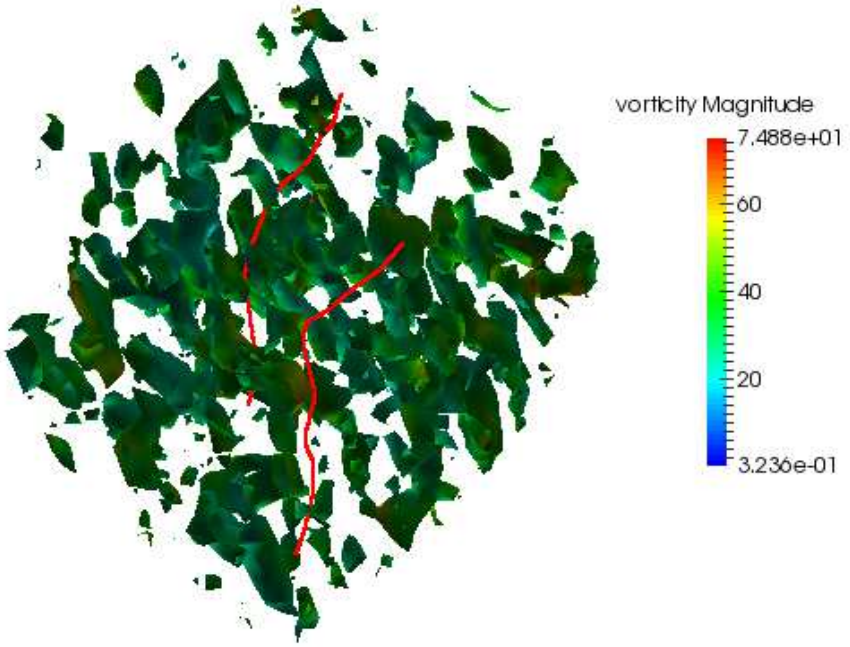

Figure 4: Location of 1D-V attractor (St=0.165 and Fr=0.49) in flow with $p = 5/3$

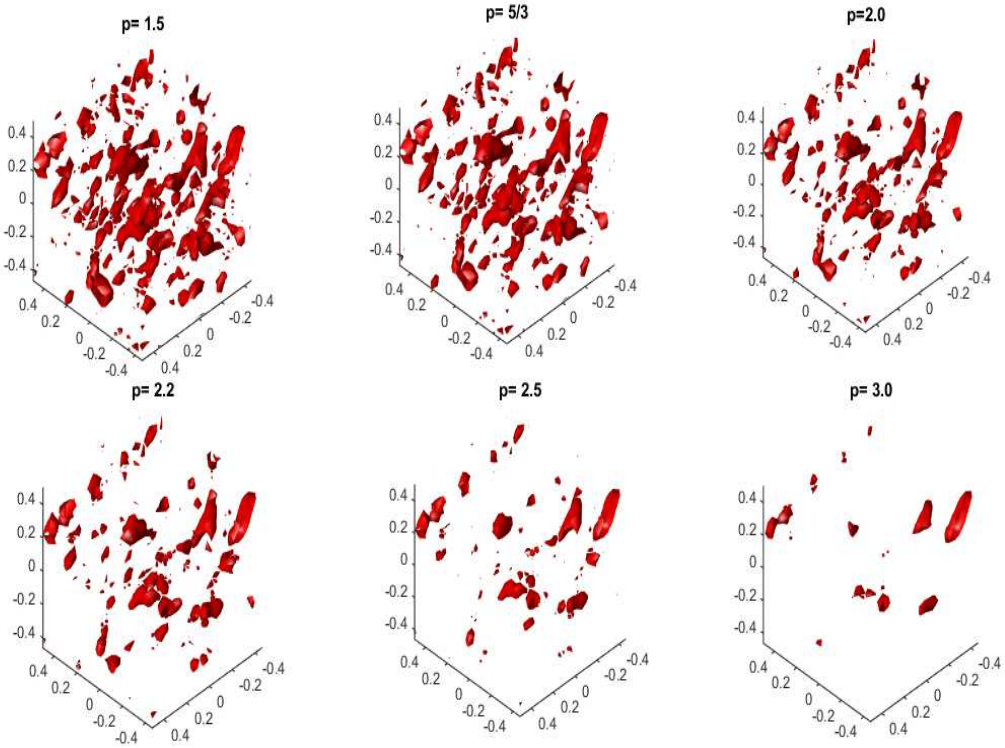

Figure 5: (a)-(f) Q-criterion isosurfaces for threshold values of Q=180 for different power laws.

4.2 Identification of attractors with non-Kolomogorov Energy Spectrum

Similar results are obtained with non-Kolmogorov power law (p) and clusters are developed in the low vorticity region. In order to identify the locations of Lagrangian attractors, isosurfaces of turbulence structures are drawn with increasing values of the power law (p). As the value of (p) increases, the smaller length scales disappear as shown in Fig. 5. As expected; the most of the energy is utilized at the larger length scales imparting random motion to the particles and as a result, the one-dimensional attractors may destroy.

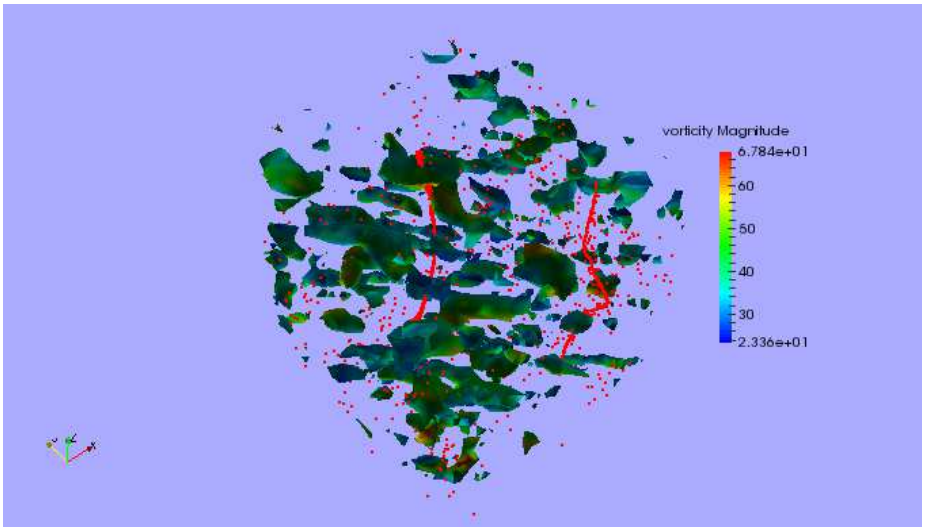

Figure 6: Location of 1D-V attractor (St=0.165 and Fr=0.49) in flow with $p = 1.5$ at t=100 s.

As an example, we present a case with 1D-V attractor with the increasing power law (p) of energy spectrum. It is noted that the attractor first moves and changes its position in the flow structure (Fig. 6-Fig. 8) with the modification and ultimately rearranges to the 3D distribution (Fig. 9). This shows different formations of turbulence structure for Kolmogorov and non-Kolmogorov energy spectra.

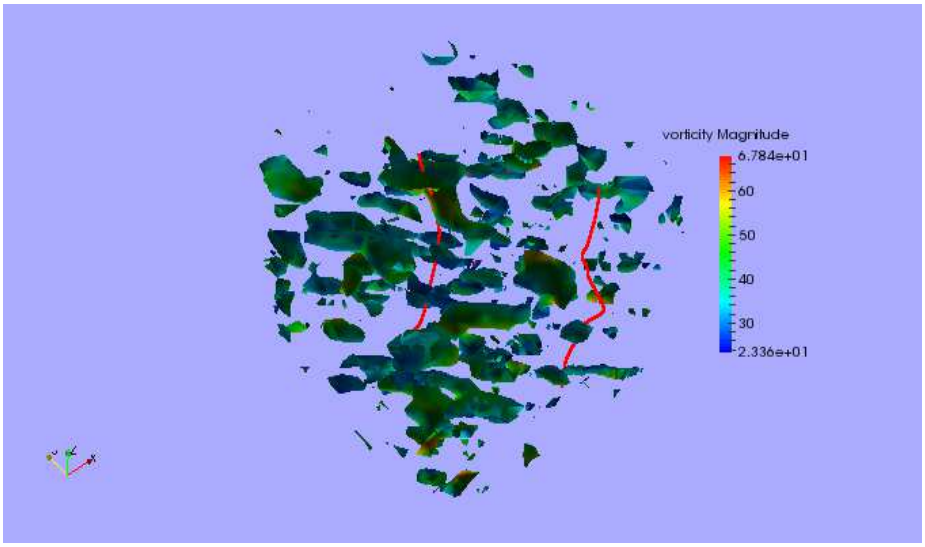

Figure 7: Location of 1D-V attractor (St=0.165 and Fr=0.49) in flow with $p = 5/3$ at t=100 s.

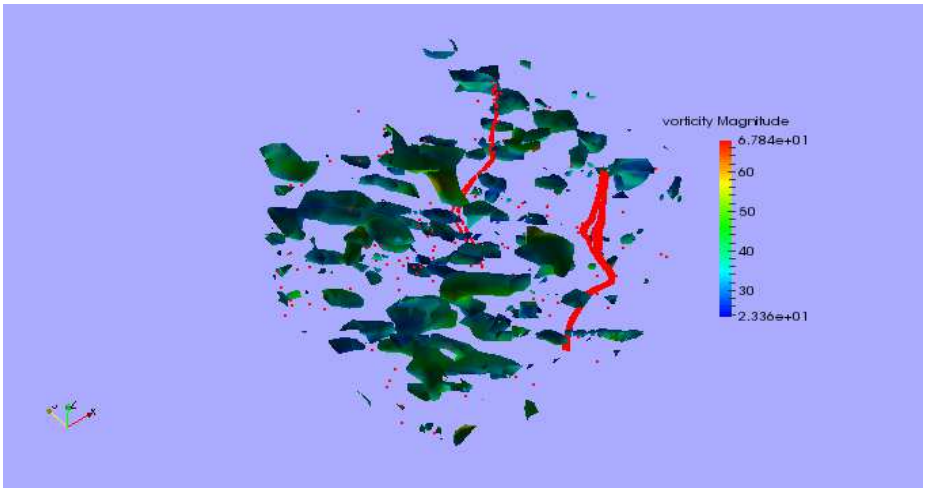

Figure 8: Location of 1D-V attractor (St=0.165 and Fr=0.49) in flow with $p = 2.0$ at t=100 s.

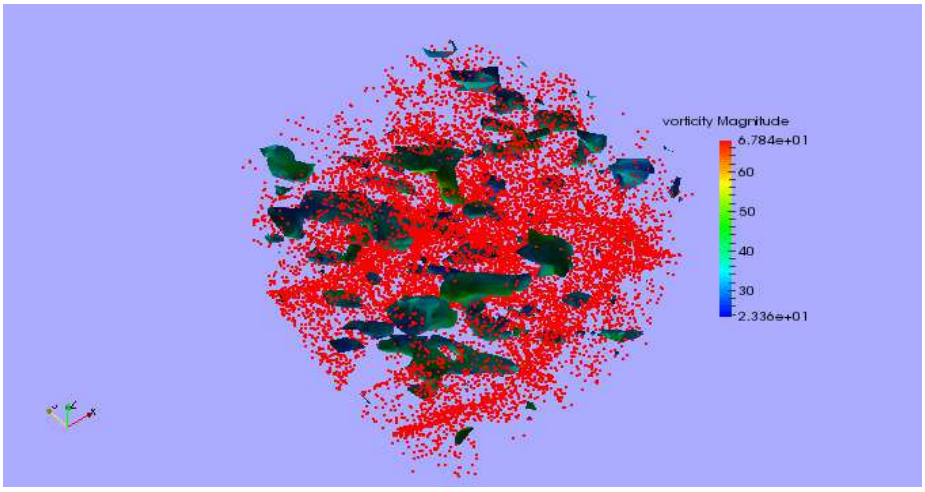

Figure 9: Location of 1D-V attractor (St=0.165 and Fr=0.49) in flow with $p = 2.5$ at t=100 s..

5 Statistical analysis of clusters' Locations

The Lagrangian attractors are tracked using visualization, but in order to confirm the locations of the particles' clusters with more meaningful approach, we perform a statistical analysis. The variations in Q-criterion distributions are studied for different shapes of attractors with Kolmogorov as well as non-Kolmogorov energy spectrum.

5.1 With Kolmogorov energy spectrum

We use the frequency distribution initial three-dimensional particles as a reference. In order to find the attractors position, we use the velocities at the attractors' final positions to calculate the Q-criterion. As Q-criterion clearly defines the strain and vorticity regions, hence it is used to detect the exact locations of the particles' attractors. For the purpose comparison with initial uniform distribution, an attractors' Q-value distributions are plotted along with the particles' initial distribution in Figs. 10- 12.

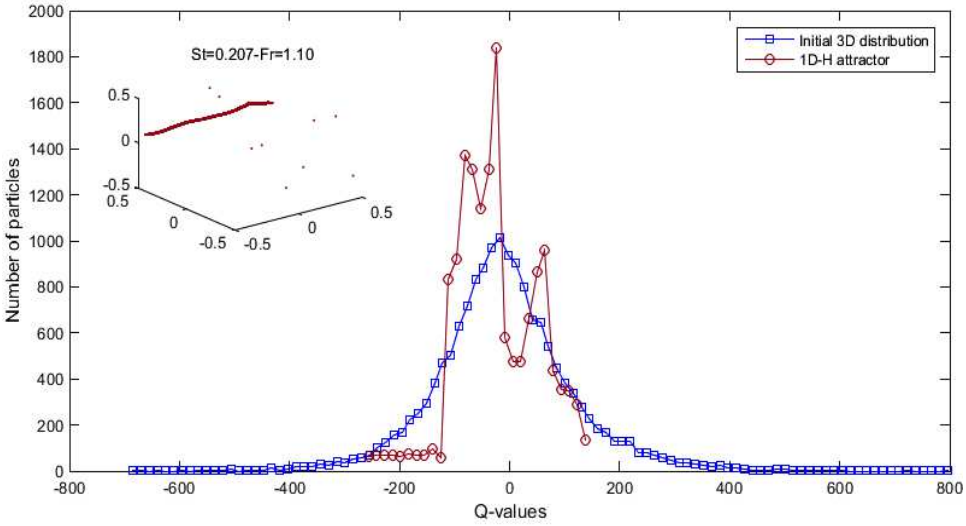

Figure 10: Q-values distribution for a horizontal attractor comparing with initial three-dimensional distribution for $p = 5/3$.

In Fig. 10, the Q-values for a 1D-H attractor can be shown and it is evident that most of the particles are on the negative side of the distribution i.e. in the strain regions with $Q < 0$. So, it is confirmed that the horizontal attractors evolve in the low vorticity regions of the flow. Similar distribution of Q-values is obtained for 1D-V attractor as shown in Fig. 11.
The difference in Q-values distributions between 1D-H and 1D-V attractors can be analyzed with careful examination of Fig. 10 and Fig. 11. In both of these cases, particles have St=0.207 with different values of Fr. For the 1D-H attractor, multi-peaks is shown in Fig. 10 describe the dominant behavior of turbulence-structure over gravity effect. on the other hand, 1D-V attractor with a single peak is the consequence of strong drift. Moreover, the Q-values distribution of the 1D-HV attractor shows features of both 1D-H and 1D-V attractors that is, we can see a spike as well as a negative skewness as shown in Fig. 12. All of three cases are put together in Fig. 13 which clearly elaborates the locations of different one-dimensional attractors in different vorticity regions.
In addition to the one-dimensional attractors, it is interesting to see the Q-values distribution of a 2D-L attractor in relation to the initial particle distribution. More precisely, we can differentiate the locations of 1D-V and 2D-L attractors on basis of vortex regions. The 1D-V attractors develop for small sized particles and they can easily move in the vortex regions. For the 2D-L attractors, the size of the particles (St) is big enough such that they cannot be trapped by the smaller length scales of vortex regions. Therefore, the Q-values distribution for the 2D-L is clearly different from the 1D-V attractor as shown in Fig. 14. Altogether,

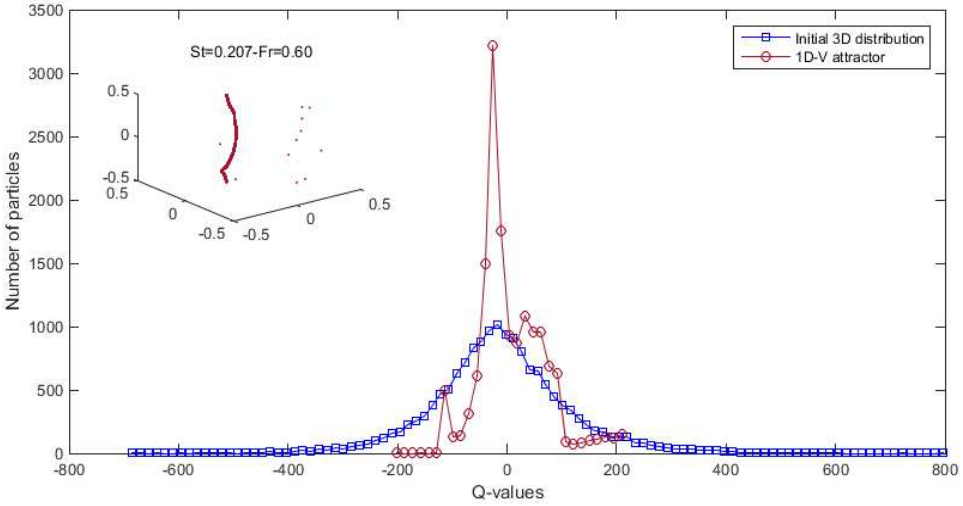

Figure 11: Q-values distribution for a vertical attractor comparing with initial three-dimensional distribution for $p = 5/3$.

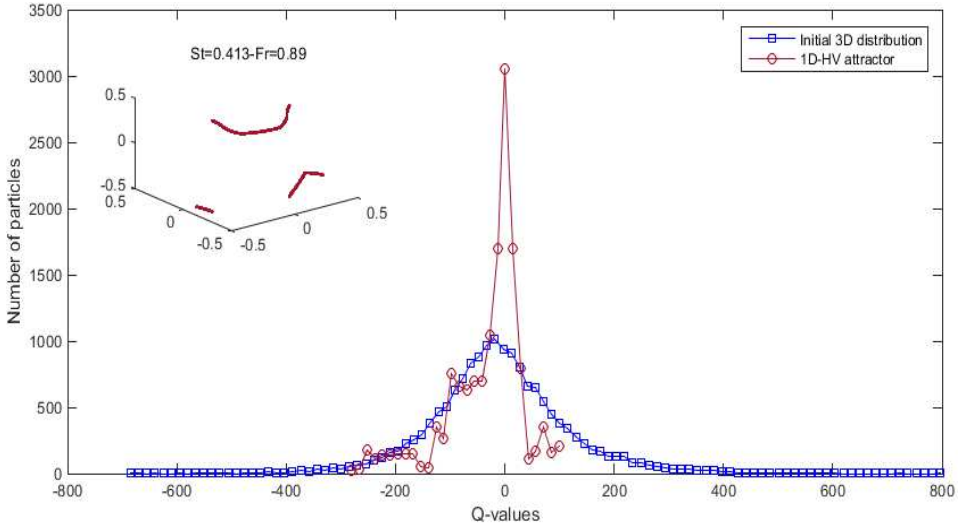

Figure 12: Distribution of Q-values at particles positions for 1D-HV attractor in comparison to initial distribution of the particles with $p = 5/3$.

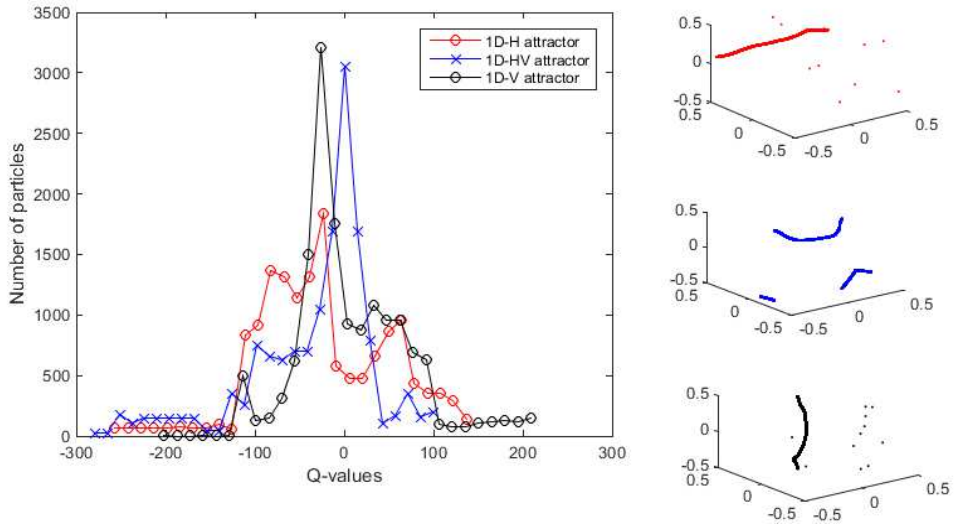

Figure 13: Comparison of Q-value distributions for different one-dimensional attractors with $p = 5/3$.

the statistical analysis is proved to be quite helpful to verify the locations of different types of attractors in vortex regions.

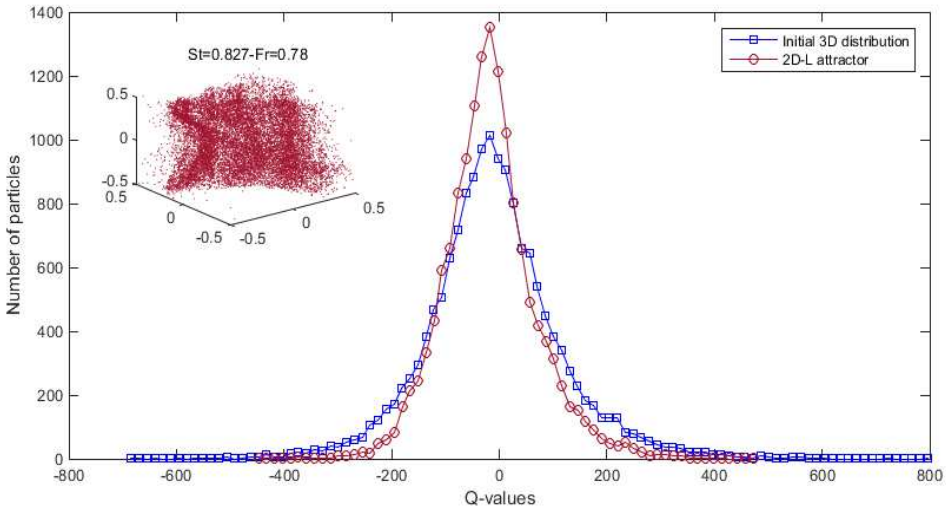

Figure 14: Distribution of Q-values at particles positions for 2D-L attractor in comparison to initial distribution of the particles with $p = 5/3$.

5.2 With non-Kolmogorov energy spectrum

Here, we apply the Q-criterion distributions by varying the power law of energy spectrum. As we have already visualized the modifications of the attractors with increasing or decreasing the p, the Q-value distribution of the particles will also differ from what we obtain with $p = 5/3$. In Fig. 15, Q-value distributions of initial particles' positions with different power law are plotted which shows that the particles have the tendency to settle in the low vorticity regions with the reduced range of scales for the higher values of p.

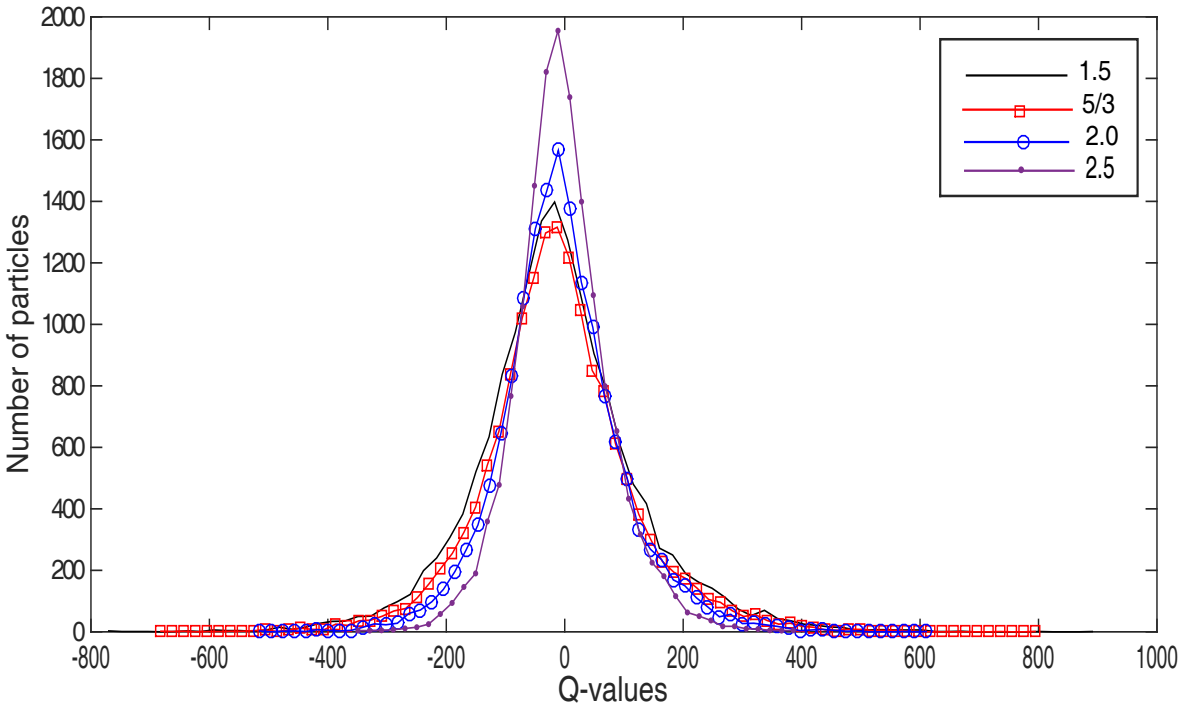

Figure 15: Q-values distributions at initial three-dimensional positions for different power laws.

We analyze the different types of Lagrangian attractor with the modified power laws. For a 1D-H attractor, the increase in p destroys the attractor. Therefore, Q- value distributions shift towards right for $p = 2.0$ and $p = 2.5$ (in Fig. 16) showing that the lighter particles tend to move randomly with the increments in p. A somewhat similar trend is noted for a 1D-V attractor as shown in Fig. 17 where we found the most of the Q-values on the negative side of distribution with $p = 5/3$. It means that there are some specially featured scales in turbulence with Kolmogorov energy spectrum which hold the particles in the strain regions.
Finally, we do not observe any kind of clear variations in the shape of the Q-values distribution for a 2D-L attractor with the modified power laws. The only noticeable change with $p = 2.5$ is a small decrement in the dispersion of distribution and this happens because of the reduction in the scales.

6 Conclusion

We have discussed in detail the clustering of inertial particles in relation to the flow structure using Q-criterion. According to visualizations and statistical analysis, we have found that the particles cluster in the flow depending on flow parameters and particles' characteristics. We present the following findings from this study:

- The visualization shows that the particles tend to cluster in the straining regions ($Q < 0$) depending on St, Fr and input energy spectrum (Kolmogorov or non-Kolmogorov).
- We found that different Lagrangian attractors (1D-H or 1D-V) develop as the result of the difference in the vorticity components of the local turbulence structures.
- The multi-peaks as shown in Fig. 10 can be considered as a distinctive feature of the 1D-H attractor revealed as the result of statistical analysis. It shows that the particles in a horizontal one-dimensional attractor may evolve in more than one types of vortex region.

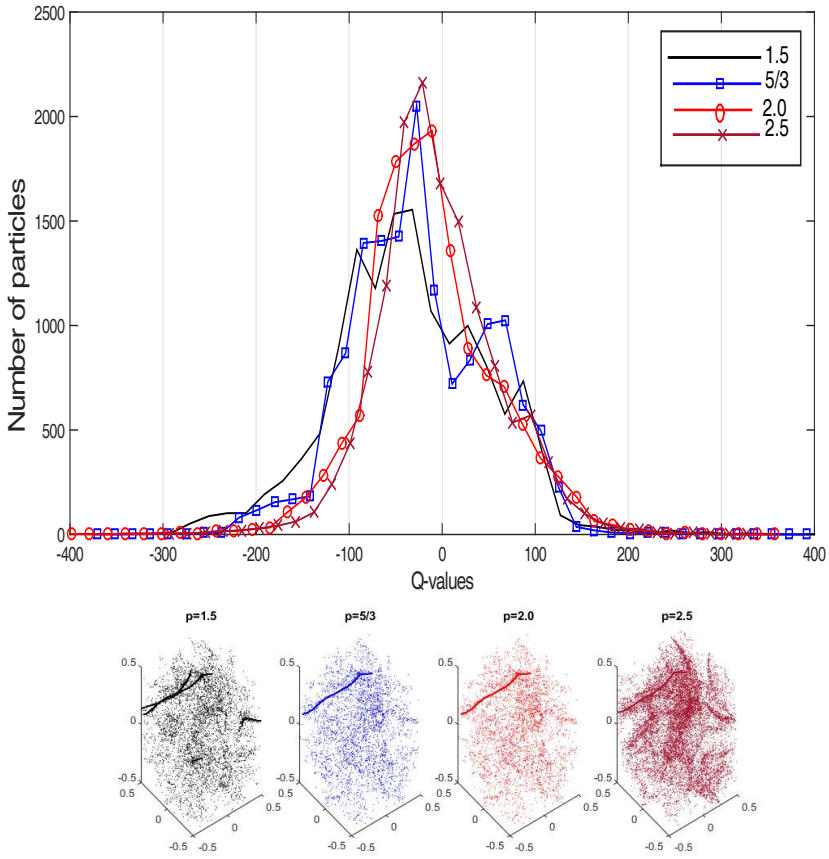

Figure 16: (top)Frequency distribution of Q-criterion at particles positions for St=0.207 and Fr=1.10 and (bottom) 3D plots for different power laws.

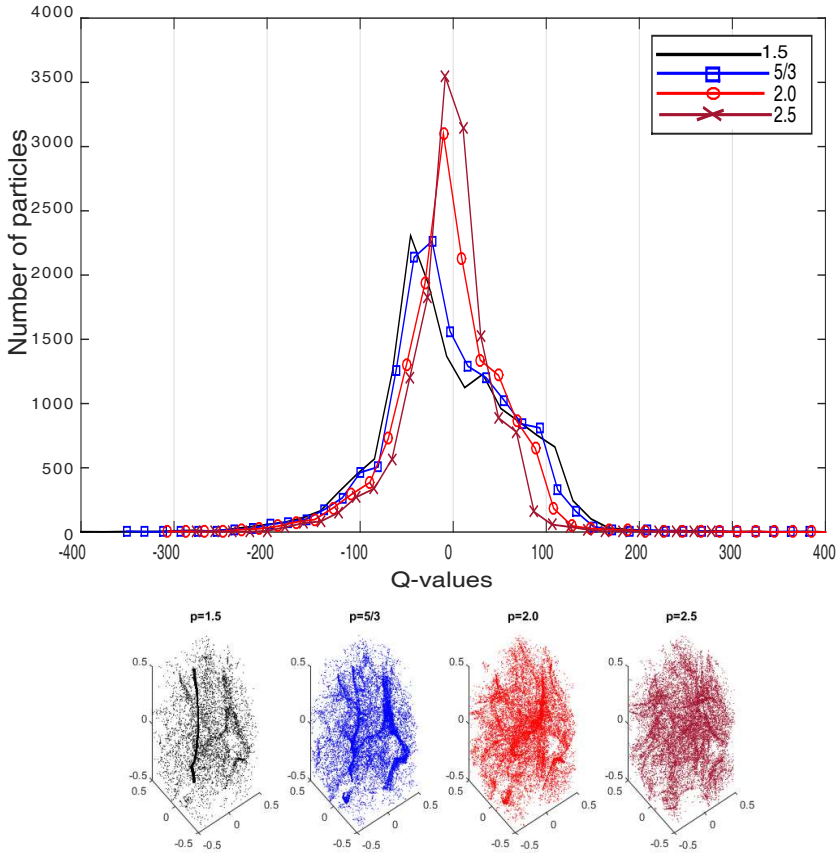

Figure 17: (top) Frequency distribution of Q-criterion at particles positions for St=0.207 and Fr=0.63 and (bottom) 3D plots for different power laws.

- The particles with $St < 0.5$ tend to accumulate in the very low vorticity regions depnding different values of Fr and can result into a 1-D attractor [8]. This is confirmed by plotting the Q-values distributions using velocity components at the particles' final positions. Our findings are also in agreement with the recent results of [16] who found that the lighter particles preferentially concentrated in the synthetic flow.
- The particles with $St > 0.5$ do not form any of the one-dimensional attractors [8] and hence the Q-value distribution of the attractor almost overlaps with that of the initial distribution of particles.
- Using the Q-criterion distributions, it is also observed that the one-dimensional attractors start juggling in the flow structures with modified power laws of the energy spectrum. While the p variations are less effective for the 2D-L structures.

References

[1] Bogdan Rosa, Hossein Parishani, Orlando Ayala, and Lian Ping Grabowski, Wojciech Wand Wang. Kinematic and dynamic collision statistics of cloud droplets from high-resolution simulations. *New J. Phys.*, 15:045032, 2013.

[2] A. Dejoan and R. Monchaux. Preferential concentration and settling of heavy particles in homogeneous turbulence. *Phys. Fluids*, 25(1):013301, 2013.

[3] Wang Y. Zhang J. Jin, G. and G. He. Turbulent clustering of point particles and finite-size particles in isotropic turbulent flows. *Industrial and engineering chesmistry research*, 52(33):11294–11301, 2013.

[4] J. Bec, H. Homann, and Samriddhi Sankar Ray. Gravity-driven enhancement of heavy particle clustering in turbulent flow. *Phys. Rev. Lett.*, 112:184501, May 2014.

[5] K. Gustavsson, S. Vajedi, and B. Mehlig. Clustering of particles falling in a turbulent flow. *Phys. Rev. Lett.*, 112:214501, May 2014.

[6] Jean-RÃľgis Angilella, Rafael D. Vilela, and Adilson E. Motter. Inertial particle trapping in an open vortical flow. *J. Fluid Mech.*, 744:183–216, 4 2014.

[7] Y. Park and C. Lee. Gravity-driven clustering of inertial particles in turbulence. *Phys. Rev. E*, 89:061004, Jun 2014.

[8] M. Farhan, F. C. G. A. Nicolleau, and A. F. Nowakowski. Effect of gravity on clustering patterns and inertial particle attractors in kinematic simulations. *Phys. Rev. E*, 91:043021, Apr 2015.

[9] F. C. G. A. Nicolleau, M. Farhan, and A. F. Nowakowski. Effect of the energy-spectrum law on clustering patterns for inertial particles subjected to gravity in kinematic simulation. *Phys. Rev. E*, 94:043109, Oct 2016.

[10] J.K. Eaton and J.R.Fessler. Preferential concentration of particle by turbulence. *Int. J. Multiphase flow*, 20:169, 1994.

[11] Kyle D. Squires and John K. Eaton. Measurements of particle dispersion obtained from direct numerical simulations of isotropic turbulence. *J. Fluid Mech.*, 226:1–35, 5 1991.

[12] Lian Ping Wang and M. R. Maxey. The motion of microbubbles in a forced isotropic and homogenous turbulence. *Applied Scientific Research*, 51:291–296, 1993.

[13] J. Bec, L. Biferale, G. Boffetta, A. Celani, M. Cencini, A. Lanotte, S. Musacchio, and F. Toschi. Acceleration statistics of heavy particles in turbulence. *J. Fluid Mech.*, 550:349–358, 3 2006.

[14] E. Calzavarini, M. Kerscher, D. Lohse, and F. Toschi. Dimensionality and morphology of particle and bubble clusters in turbulent flow. *J. Fluid Mech.*, 607:13–24, 7 2008.

[15] S. W. Coleman and J. C. Vassilicos. A unified sweep-stick mechanism to explain particle clustering in two- and three-dimensional homogeneous, isotropic turbulence. *Phys. Fluids*, 21(11), 2009.

[16] Christopher Nilsen and Helge I. Andersson. Mechanisms of particle clustering in gaussian and non-gaussian synthetic turbulence. *Phys. Rev. E*, 90:043005, Oct 2014.

[17] F. W. Elliott and A. J. Majda. Pair dispersion over an intertial range spanning many decades. *Phys. Fluids*, 8(4):1052–1060, 1996.

[18] N. A. Malik and J. C. Vassilicos. A lagrangian model for turbulent dispersion with turbulent-like flow structure: comparison with dns for two-particle statistics. *Phys. Fluids*, 11(6):1572–1580, 1999.

[19] F. C. G. A. Nicolleau and A. F. Nowakowski. Presence of a richardson's regime in kinematic simulations. *Phys. Rev. E*, 83:056317, May 2011.

[20] A. Abou-El-Azm and F. Nicolleau. Dispersion of heavy particle sets in an isotropic turbulence using kinematic simulation. *Phys. Rev. E*, 78(1):0616310, 2008. doi:10.1103/PhysRevE.78.016310.

[21] R. Gatignol. The faxen formulae for a rigid particle in an unsteady non-uniform stokes flow. *J. Mech. Theor. Appl.*, 1(2):143–160, 1983.

[22] M. R. Maxey and J. J. Riley. Equation of motion for a small rigid in a nonuniform flow. *Physics of Fluids*, 26(4):883–889, 1983.

[23] H.J. J. Woittiez, E. J. P.; Jonker and L. M. Portela. On the combined effects of turbulence and gravity on droplet collisions in clouds: A numerical study. *J. Atmos. Sci.*, 66(7):1926–1943, 2008.

[24] J.C.R. Hunt, A.A. Wray, and P. Moin. Eddies, stream, and convergence zones in turbulent flows. *Center for Turbulence Research Report CTR-S88*, 0:193–208, 1988.